THE JOURNAL OF PHYSICAL CHEMISTRY B

Article

pubs.acs.org/JPCB

Reactive Conformation of the Active Site in the Hairpin Ribozyme Achieved by Molecular Dynamics Simulations with ε/ζ Force Field Reparametrizations

Vojtěch Mlýnský,[†] Petra Kührová,[†] Marie Zgarbová,[†] Petr Jurečka,[†] Nils G. Walter,[‡] Michal Otyepka,[†] Jiří Šponer,[†,§,∥] and Pavel Banáš*[,†,§]

[†]Regional Centre of Advanced Technologies and Materials, Department of Physical Chemistry, Faculty of Science, Palacky University, tr. 17 listopadu 12, 771 46 Olomouc, Czech Republic

[‡]Department of Chemistry, Single Molecule Analysis Group, University of Michigan, 930 North University Avenue, Ann Arbor, Michigan 48109-1055, United States

[§]Institute of Biophysics, Academy of Sciences of the Czech Republic, Kralovopolska 135, 612 65 Brno, Czech Republic

[∥]CEITEC − Central European Institute of Technology, Masaryk University, Campus Bohunice, Kamenice 5, 625 00 Brno, Czech Republic

Supporting Information

ABSTRACT: X-ray crystallography can provide important insights into the structure of RNA enzymes (ribozymes). However, the details of a ribozyme's active site architecture are often altered by the inactivating chemical modifications necessary to inhibit self-cleavage. Molecular dynamics (MD) simulations are able to complement crystallographic data and model the conformation of the ribozyme's active site in its native form. However, the performance of MD simulations is driven by the quality of the force field used. Force fields are primarily parametrized and tested for a description of canonical structures and thus may be less accurate for noncanonical RNA elements, including ribozyme catalytic cores. Here, we show that our recent reparametrization of ε/ζ torsions significantly improves the description of the hairpin ribozyme's scissile phosphate conformational behavior. In addition, we find that an imbalance in the force field description of the nonbonded interactions of the ribose 2′-OH contributes to the conformational behavior observed for the scissile phosphate in the presence of a deprotonated G8^{-}. On the basis of the new force field, we obtain a reactive conformation for the hairpin ribozyme active site that is consistent with the most recent mechanistic and structural data.

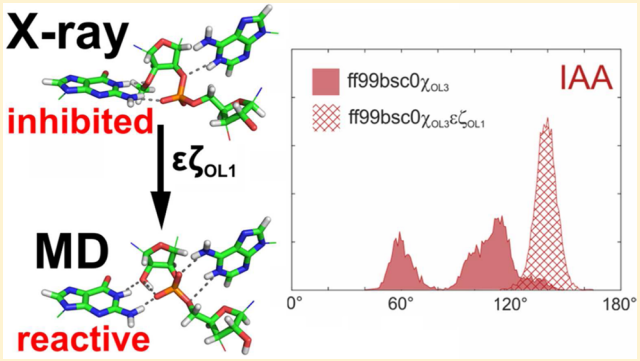

INTRODUCTION

RNA enzymes, or ribozymes, are catalytic noncoding RNAs.[1,2] The small ribozymes, e.g., the hairpin ribozyme, are autocatalytic RNA molecules that catalyze site-specific cleavage of their own sugar−phosphate backbone.[1−4] This reaction participates in several biological processes such as self-splicing processes or replication of viral satellite RNAs.[5−8] Studies of ribozyme mechanisms are complicated by difficulties in crystallizing the precleavage forms due to their inherent reactivity.[1,9] Therefore, chemical modifications are usually introduced into the active site to inhibit self-cleavage in structural studies, often altering a catalytically important nucleotide. A common approach is inactivation of the native 2′-OH nucleophile by replacing it with a 2′-OMe group or 2′-H hydrogen, yielding methoxy or deoxy modifications, respectively.[10] Therefore, although X-ray crystallography can provide decisive insights into the structures of ribozymes, the required modifications often perturb the conformation of the active site and complicate interpretation of the structural data.[1,11−13] In addition, RNA crystal structures deposited in the Protein Data Bank (PDB) may suffer from local geometrical, conformational, and steric errors that need to be corrected.[14]

Molecular dynamics (MD) simulations can complement experimental structures of ribozymes, e.g., by modeling the arrangement of their active sites in the reactive form.[12,15−21] Sufficiently long simulations starting from the crystal structure but without the modifications should relax the active site to help correct local errors and eliminate the biases associated with any inhibiting modification.[12,20,22−25] Thus, MD simulations effectively are able to model and potentially refine the

Received: December 3, 2014
Revised: February 16, 2015
Published: February 18, 2015

DOI: 10.1021/jp512069n
J. Phys. Chem. B 2015, 119, 4220−4229

native (reactive) conformation of the active site on the basis of available crystallographic data. To fully live up to their potential, however, MD simulations need to overcome two potentially limiting factors: (i) approximations of the force field (in the case of RNA, mainly the description of the noncanonical conformation of the sugar−phosphate backbone)[26−29] and (ii) limited sampling, which may be insufficient to overcome the errors and biases of the starting structure.[20,30−33] The former limitation is indeed critical for an accurate description of the conformation of the scissile phosphate as the in-line-attack (IAA) conformation required for the self-cleavage reaction can only be achieved by noncanonical and relatively rarely populated conformations of the sugar−phosphate backbone, particularly via specific combinations of the ε/ζ torsions and the ribose pucker. Empirical force fields are usually parametrized and tested with canonical structures in mind and therefore do not always provide a balanced description of noncanonical regions, including conformations of the scissile phosphates in ribozymes.

Like other small ribozymes, the hairpin ribozyme does not require metal ions in the active site to achieve catalysis.[4,10,34,35] A wealth of mechanistic data has shown that two key nucleobases are required for catalysis: guanine 8 (G8) and adenine 38 (A38).[13,36−45] These experimental measurements, together with theoretical calculations, strongly support the hypothesis that A38 is protonated and acts as a general acid by protonation of the O5′ leaving group.[13,22,46−51] The G8 may be deprotonated and act as a general base by accepting a proton from the 2′-OH nucleophile and/or it may assist in attack of the 2′-OH group on the scissile phosphate by electrostatic stabilization of the transition state (Scheme 1).[46,50−52] Thus,

Scheme 1. A38H$^+$/G8$^-$ General Acid/Base Mechanism Suggested for Self-Cleavage of the Sugar−Phosphate Backbone of the Hairpin Ribozyme

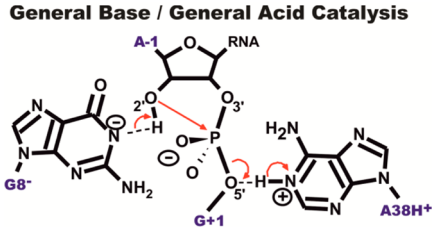

one set of mechanistic data suggests that the reactive form of the hairpin ribozyme may be a rarely populated protonation state that is, however, sufficiently reactive to compensate for the thermodynamic penalty of being a minor protonation state. This hypothesis has been supported by hybrid quantum chemical molecular mechanical (QM/MM) calculations.[51,53] Such a state is expected to include A-1(2′-OH)···G8$^-$(N1) and A38H$^+$(N1H)···G+1(O5′) hydrogen bonds (H-bonds) accompanied by a high value of the IAA, i.e., the A-1(O2′)−G+1(P)−G+1(O5′) angle.

Despite the progress in understanding hairpin ribozyme self-cleavage, several questions remain concerning the catalytic mechanism. In particular, until now neither experimental structural data nor MD simulations have revealed any conformation of the hairpin ribozyme active site that would be fully preorganized for catalysis. Most crystal structures of the hairpin ribozyme precursor are inhibited by a A-1(2′-OMe) methoxy modification and consistently exhibit a C2′-endo pucker for the 2′-methoxylated A-1 ribose.[38,54−56] In contrast, MD simulations (using the older *ff*99[57,58] and *ff*99bsc0[59] versions of the AMBER force field) of the native precursor state, i.e., with a starting structure based on the 2′-OMe crystal structures but with native 2′-OH ribose, showed a rapid repuckering of the A-1 ribose from the original C2′-endo to C3′-endo, i.e., to the ribose pucker typical for A-form RNA duplexes. This caused a significant displacement of the 2′-OH nucleophile, significant decrease of the IAA (Figures 1 and 2A),

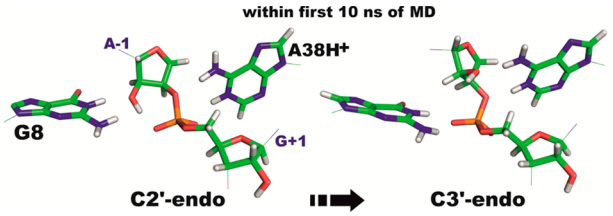

Figure 1. Swift repuckering of A-1 ribose observed in MD simulations of the hairpin ribozyme with the default *ff*99bsc0χ_{OL3} force field, in which the nucleophilic 2′-OH group is displaced from G8(N1) to A38(N6).[12,22]

and a loss of the G8(N1H)···A-1(O2′) H-bond.[12,22] This simulation behavior was tentatively explained as a consequence of removal of the 2′-OMe mutation.[22] However, we could not rule out that the force field may be biased to excessively stabilize the canonical C3′-endo pucker. Recently, substantial reparametrizations of the torsional terms of the AMBER nucleic acids force field were suggested (for a review, see ref 60). The RNA-specific χ_{OL3} modification[61] is essential to prevent high-anti χ abnormalities of the RNA structures and also improves description of the χ *syn* region. The $\varepsilon\zeta_{OL1}$ modification was then introduced to improve the helical twist and the BI−BII balance of B-DNA and the structural dynamics of DNA quadruplexes.[62] The latter reparametrization could in principle improve also the performance of RNA simulations, although substantial testing for a wide range of systems will be needed to confidently utilize it for RNA.

Here, we test the possibility that a force field bias affects details of the conformational dynamics of the active site observed in older force fields and that the behavior can be improved with the above-noted recent force field versions, which until now have not been used for the hairpin ribozyme. Indeed, we show that the ε/ζ DNA backbone torsion modification[62] coupled with the essential χ modification[61] significantly improves the description of the backbone conformation of the hairpin ribozyme active site in the presence of a canonical G8. In addition, we find that the departure of the deprotonated G8$^-$ from the active site is driven by the orientational preferences of the A-1(2′-OH) hydroxyl. Finally, we use more accurate QM/MM calculations in the presence of the deprotonated G8$^-$ to benchmark the force field and propose directions for future force field improvements.

METHODS

Setup for MD Simulations. Starting structures were based on the crystal structure of a minimal, junctionless hairpin ribozyme grown at pH 6.0 and determined at 2.05 Å resolution (PDB ID 2OUE, original PDB code 1ZFR).[55] We tested two different protonation forms of G8 at the active site, i.e., a canonical G8 and an N1-deprotonated G8$^-$. The canonical

DOI: 10.1021/jp512069n
J. Phys. Chem. B 2015, 119, 4220−4229

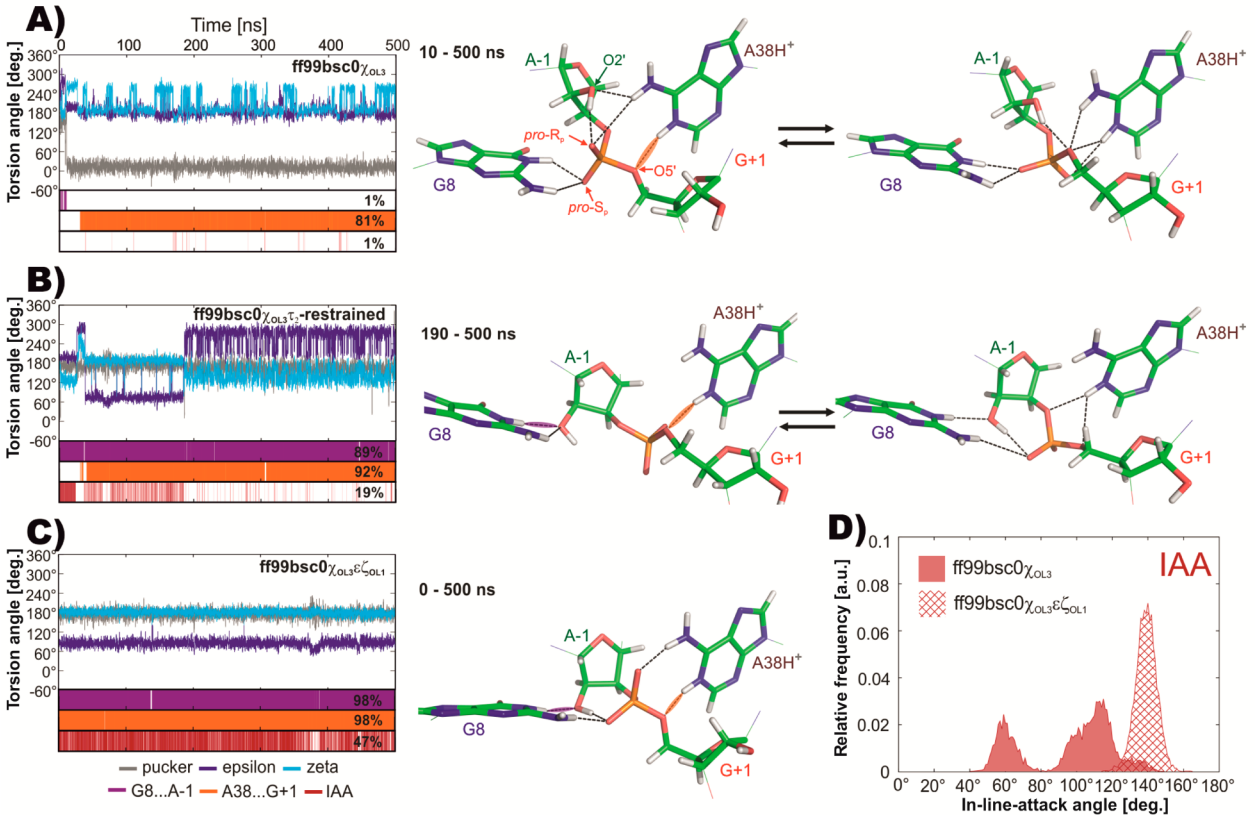

Figure 2. Structural dynamics of the active site as observed in 500 ns MD simulations (A) with the default *ff*99bsc0χ_{OL3} AMBER RNA force field, (B) with the same force field with restrained A-1 C2′-endo ribose pucker, and (C) in an unrestrained simulation using the *ff*99bsc0$\chi_{OL3}\varepsilon\zeta_{OL1}$ force field. The time courses of the A-1 pucker, ε, and ζ torsions that together determine the conformation of the scissile phosphate are shown in the plots on the left; the occurrences of G8(N1H)···A-1(O2′) and A38H$^+$(N1H)···G+1(O5′) H-bonds (with heavy atom distance below 3.5 Å) and favorable IAA (above 140°) are shown by the bars at the bottom of the plots with percent of total population indicated. The structures illustrate the dominantly populated active site conformations during the respective MD simulations. (D) Histograms of IAA (A-1(O2′)−G+1(P)−G+1(O5′) from the *ff*99bsc0χ_{OL3} and *ff*99bsc0$\chi_{OL3}\varepsilon\zeta_{OL1}$ simulations.

form of G8 was used for three different MD simulations: (i) an unrestrained simulation with the *ff*99bsc0χ_{OL3} force field (AMBER *ff*99 Cornell et al. force field[57,58] corrected by the Barcelona α/γ[59] and Olomouc χ_{OL3}[61] reparametrizations), (ii) a *ff*99bsc0χ_{OL3} simulation with soft flat-well restraint on the A-1 ribose pucker, and (iii) an unrestrained simulation with the *ff*99bsc0$\chi_{OL3}\varepsilon\zeta_{OL1}$ force field.[62] The flat-well potential restraint was applied on the A-1 ribose pucker: the τ_2 torsion (C1′−C2′−C3′−C4′) was unrestrained below the value of −20°, harmonic restraining potential with a force constant of 10 kcal/(mol·rad^2) was applied from −20° to 0°, and a linear extension of this potential was used for positive values of the τ_2 dihedral. Such a restraining potential retains the C2′-endo pucker conformations while providing a rather soft penalization for the O4′-endo and C3′-endo puckers (with an ∼3−4 kcal/mol bias disfavoring a C3′-endo pucker).

Additionally, seven *ff*99bsc0$\chi_{OL3}\varepsilon\zeta_{OL1}$ simulations were performed with a deprotonated G8$^-$: (i) three unrestrained simulations with various ionic conditions (see below), (ii) simulation with distance restraint applied to the G8$^-$(N2)···U+2(O4) H-bond, (iii) simulation with distance restraint applied to G8$^-$(N1)···A-1(O2′), and finally (iv) two simulations with flat-well restraint applied to the orientation of A-1(2′-OH) hydroxyl (C1′−C2′−O2′−HO2′ torsion), the first with restraint applied only for the initial 10 ns and the second restraining the dihedral for the entire simulation. All these restraints aimed to stabilize the G8$^-$ in the active site to investigate the reasons for its expulsion from the active site in unrestrained simulations (see the Supporting Information for details).

In the first two simulations without $\varepsilon\zeta_{OL1}$ correction, the hairpin ribozyme was net-neutralized with Na$^+$ counterions (well-depth ε = 0.0028 kcal/mol, radius R = 1.8680 Å)[63] and immersed in a rectangular water box with a layer of TIP3P water molecules at least 10.0 Å thick around the RNA solute. The starting structures of the simulations with $\varepsilon\zeta_{OL1}$ correction were based on a representative snapshot from the *ff*99bsc0χ_{OL3} simulation that used a soft flat-well restraint to keep the active site in reactive conformations. In these simulations, we used a slightly larger simulation box with a layer of TIP3P water molecules at least 15.0 Å thick around the RNA solute and ∼0.2 M KCl excess salt; exceptions were two additional unrestrained simulations with G8$^-$, wherein we tested the effect of ionic conditions on the behavior of the deprotonated G8$^-$ nucleotide using ∼0.2 M NaCl excess salt or net-neutralizing K$^+$ concentrations (K$^+$ well-depth ε = 0.1937 kcal/mol, radius R = 1.705 Å; Na$^+$ well-depth ε = 0.0874 kcal/mol, radius R = 1.369 Å; Cl$^-$ well-depth ε = 0.0355 kcal/mol, radius R = 2.513 Å).[64] In all simulations, the solute−solvent system was minimized prior to MD simulation as follows. Minimization of the ribozyme hydrogen atoms was followed by minimization of counterions and water molecules, while the positions of the RNA molecule remained constrained. Subsequently, all RNA atoms were frozen and the solvent molecules with counterions

DOI: 10.1021/jp512069n
J. Phys. Chem. B 2015, 119, 4220−4229

were allowed to move during a 500 ps long MD run under *NpT* conditions (p = 1 atm., T = 298.16 K) to relax the total density. After this, the solute and nucleobases were relaxed by several minimization runs with decreasing force constants applied to the sugar−phosphate backbone atoms. After relaxation was completed, the system was heated in two steps: the first step involved heating under *NVT* conditions for 100 ps, whereas the second step involved density equilibration under *NpT* conditions for an additional 100 ps. The particle-mesh Ewald (PME) method for treating electrostatic interactions was used, and all simulations were performed under periodic boundary conditions on the *NpT* ensemble at 298.16 K using the weak-coupling Berendsen thermostat.[65] The SHAKE algorithm was applied to all bonds containing hydrogen atoms. The length of each of the three simulations involving a canonical G8 (i.e., unrestrained *ff*99bsc0χ_{OL3}, restrained *ff*99bsc0χ_{OL3}, and unrestrained *ff*99bsc0$\chi_{OL3}\varepsilon\zeta_{OL1}$) was 500 ns, and the length of the remaining simulations with a deprotonated G8$^-$ was 100 ns for each of three unrestrained simulations and 50 ns for others, except for one that was extended to 500 ns with the A-1(2′-OH) orientation restrained over the entire simulation.

Setup for QM/MM Calculations. QM/MM calculations were used as a benchmark to test the accuracy of the force field description of 2′-OH orientation within the active site. We used the same combined quantum mechanical/molecular mechanical (QM/MM) setting as reported in refs 51 and 53 for the dianionic reaction pathway (with deprotonated guanine G8$^-$ and protonated A38H$^+$ adenine). A two-layer ONIOM method[66] with electronic embedding implemented in Gaussian09[67] was used for the QM/MM calculations. The MM region was treated by the *ff*99bsc0$\chi_{OL3}\varepsilon\zeta_{OL1}$ force field.[57−59,61,62] The QM region was described by the density functional theory (DFT) MPW1K functional[68,69] with the 6-31+G(d,p) basis set.

The QM region (63 atoms) comprised the A-1/G+1 sugar−phosphate backbone and the N9-methyl-capped nucleobases G8$^-$ and A38H$^+$ (see Figure 1B in ref 51). Dangling bonds at the interface between the QM and MM regions were capped by hydrogen atoms. In all QM/MM calculations, the ribozyme was surrounded by a ∼10 Å thick layer of water molecules forming a water droplet. The initial structure including the initial positions of counterions for the QM/MM calculation was taken from a representative snapshot of the MD simulation using the *ff*99bsc0$\chi_{OL3}\varepsilon\zeta_{OL1}$ force field with canonical G8 (see the Supporting Information for structure). A ∼5 Å thick layer of water molecules on the surface of the droplet and counterions outside the droplet were fixed during QM/MM calculation to prevent reorganization of the hydrogen bonding network on the top of the water droplet that might result in discontinuities of the potential energy unrelated to the structural changes in QM region. The entire system contained ∼13 000 atoms, ∼5200 of which were fixed; i.e., the majority of atoms were unconstrained.

The energy profile of the 2′-OH group rotation was explored by a flexible scan modifying the A-1(C1′)−A-1(C2′)−A-1(O2′)−A-1(HO2′) dihedral. Scans were performed with 10° steps using flexible scanning; i.e., all remaining degrees of freedom relaxed at each point (except for the fixed atoms indicated above). The MM scan aimed to test the accuracy of the force field description (with the QM/MM data used as the benchmark) was performed on the same system (containing ∼13 000 atoms) as the QM/MM calculations using Gaussian09.[67] In the MM scans we used the *ff*99bsc0χ_{OL3} and *ff*99bsc0$\chi_{OL3}\varepsilon\zeta_{OL1}$ force fields as well as the *ff*99bsc0$\chi_{OL3}\varepsilon\zeta_{OL1}$ force field with modified van der Waals parameters of phosphate oxygens originally suggested by Case et al. for phosphorylated amino acids.[70]

RESULTS AND DISCUSSION

We performed three 500 ns long and seven (three 100 ns long, three 50 ns long, and one 500 ns long) explicit solvent MD simulations of the hairpin ribozyme with canonical and deprotonated guanine G8, respectively, using different force fields and simulation settings (see Methods). We aimed to carefully analyze the effects of the approximate force field description on the structural dynamics of the hairpin ribozyme active site and identify the force field biases. The *ff*99bsc0χ_{OL3} version of the AMBER Cornell et al. force field (internally abbreviated as *ff*10, *ff*12, or somewhat confusingly *ff*14SB in the recent AMBER code versions)[71] is a well-performing and the most widely tested RNA force field. The χ_{OL3} is a crucial RNA correction of the older *ff*99/*ff*99bsc0 force field as it prevents formation of spurious ladderlike RNA structures.[22,26,61] To investigate the role of the A-1 ribose pucker in the structural dynamics of the hairpin ribozyme active site, we performed an unrestrained *ff*99bsc0χ_{OL3} simulation with the canonical form of G8 and then performed a simulation with an applied dihedral restraint on the τ_2 torsion of the A-1 ribose ring to maintain its C2′-endo pucker (for details see Methods). The third simulation with a canonical G8 and all simulations with a deprotonated G8$^-$ used the *ff*99bsc0$\chi_{OL3}\varepsilon\zeta_{OL1}$ force field corrected by the Olomouc $\varepsilon\zeta_{OL1}$[62] reparametrization of the ε/ζ torsion angles.

Rapid Reconformation of the A-1 Ribose During MD Simulations with a Canonical G8. Consistent with previous *ff*99bsc0 simulations,[22] we observed a rapid repuckering of the A-1 ribose from the C2′-endo to the C3′-endo conformation when the *ff*99bsc0χ_{OL3} force field was used, leading to loss of the G8(N1H)···A-1(O2′) H-bond and a decrease of the IAA (Figure 1). In the C3′-endo state, we observed fast fluctuations between two conformations of the scissile phosphate (Figure 2A) with only a marginal population of conformations suitable for the self-cleavage reaction, i.e., those having higher values (above ∼140°) of the IAA accompanied by A38H$^+$(N1H)···G+1(O5′) and G8(N1H)···A-1(O2′) H-bonds (Figure 2D). In the earlier MD studies we hypothesized, on the basis of the available structural data, that the swift A-1 repuckering was related to the removal of the 2′-methoxy modification in the active site.[12,22] This was because the available precleavage crystal structures with A-1(2′-OMe) modification had a C2′-endo pucker of the A-1 ribose,[38,54,55,72] whereas those bearing the native A-1(2′-OH) group (albeit being modified by nucleobase replacements at the critical positions of either G8 or A38) suggested variable sugar puckers, including O4′-exo, C3′-exo, O4′-endo, and C3′-endo.[13,54,55] Thus, although experimental data clearly supported a C2′-endo ribose pucker in structures with A-1(2′-OH) modification, an ambiguous ribose pucker was observed in structures with the native A-1(2′-OH) ribose.

We then performed restrained *ff*99bsc0χ_{OL3} simulation biased in favor of the C2′-endo pucker of the A-1(2′-OH) ribose. After a few tens of nanoseconds, the scissile phosphate flipped into a conformation well-suited for catalysis. This allowed the firm H-bonds between the scissile phosphate and the catalytically important nucleobases G8/A38H$^+$, namely G8(N1H)···A-1(O2′), G8(N2H)···G+1(pro-S$_P$),

DOI: 10.1021/jp512069n
J. Phys. Chem. B 2015, 119, 4220−4229

A38H$^+$(N1H)···G+1(O5′), and A38H$^+$(N6H)···G+1(pro-R_P). Furthermore, high values of the IAA were populated, with a mean value of ∼140° and fluctuations up to 170° (Figure 2D). Nonetheless, the simulation maintained this geometry only for ∼150 ns. Then the scissile phosphate lost the reactive conformation and adopted another fluctuating (bistable) state (Figure 2B). Deeper analysis of the trajectory indicates that the rarity of observing a reactive conformation in earlier simulations may have been caused by an inaccurate description of the ribose pucker or ε/ζ torsions (or a combination of both). This is because the reactive conformation of the active site temporarily sampled in our *ff*99bsc0χ_{OL3} simulation with restrained C2′-endo pucker was characterized by a +gauche/trans (g+/t) conformation of the A-1 ε/ζ torsions. This is a rare, noncanonical conformation of the RNA sugar−phosphate backbone that does not correspond to any annotated suite in the database of RNA backbone conformations.[73,74] However, some occurrences of this sugar−phosphate backbone can be found in the PDB database (Figure 3B in ref 73). Formation of such a very rare backbone topology in the catalytic center of a ribozyme would not be surprising.

Reparametrized ε/ζ Torsions Have a Significant Effect on the Conformation of the Sugar−Phosphate Backbone and the A-1 Pucker. Recently, a reparametrization of the ε/ζ torsions was introduced and shown to significantly improve the simulation behavior of DNA systems,[62] in particular the balance between the populations of BI and BII states and the helical twist in B-DNA. Notably, this reparametrization stabilizes the ε/ζ g+/t conformation of the sugar−phosphate backbone relative to the earlier force field versions (Figure S1 in the Supporting Information). As the Cornell et al. force field variants (without the $\varepsilon\zeta_{OL1}$ correction) share the same ε/ζ parameters for both DNA and RNA, we expected that the $\varepsilon\zeta_{OL1}$ reparametrization may also affect RNA as it is supposed to generally improve the description of the conformational behavior of the sugar−phosphate backbone in both DNA and RNA. Initial testing of the $\varepsilon\zeta_{OL1}$ correction on a canonical A-RNA duplex yielded stable simulations where the simulated dihedral and nucleobase structural parameters corresponded well with a crystal structure reference.[62] Thus, we decided to test the $\varepsilon\zeta_{OL1}$ correction for the hairpin ribozyme.

With the *ff*99bsc0$\chi_{OL3}\varepsilon\zeta_{OL1}$ force field we indeed found remarkable improvement of the structural dynamics of the hairpin ribozyme active site. In particular, when started from the reactive state temporarily sampled by the restrained simulation (see above), the hairpin ribozyme maintained the reactive active site conformation including the high values of the IAA over the entire 0.5 μs simulation (Figure 2C). It is worth noting that in this simulation, the A-1 ribose pucker dominantly populated the C2′-endo conformation (despite the fact that we did not apply any restraining potential). Thus, it seems that the preference for the C3′-endo conformation in the *ff*99bsc0χ_{OL3} and prior *ff*99bsc0[22] and *ff*99[12,22] simulations was dictated by the local conformation of the scissile phosphate. Once the ε/ζ torsions adopt the g+/t conformation upon introduction of the $\varepsilon\zeta_{OL1}$ correction, the A-1 ribose stably fluctuates in the C2′-endo region.

The simulations indicate that the pucker is a rather soft (passive) structural parameter, at least in this particular case. The pucker preference appears to follow the local conformation of the attached downstream phosphate, particularly the values of its ε/ζ torsions. Therefore, we suggest that the $\varepsilon\zeta_{OL1}$ correction may be essential for simulating the proper structural dynamics of the scissile phosphates in ribozymes. In contrast to the earlier simulations[11,12,22] and similarly in contrast to the available structural data,[13,38,54,55] the *ff*99bsc0$\chi_{OL3}\varepsilon\zeta_{OL1}$ force field spontaneously stabilizes geometry of the catalytic center that appears to be well-poised to support the catalysis. Previous crystal structures of the hairpin ribozyme with an inhibiting A-1(2′-OMe) modification[13,38,54,55] revealed t/t states of the ε/ζ torsions. In such a conformation, the scissile phosphate adopts a geometry where G8(N2)···G+1(pro-S_P) and A38(N6)···G+1(pro-R_P) H-bonds are not established and the key A38(N1)···G+1(O5′) interaction is weakened. ε/ζ t/t geometries similar to this (with a modest shift toward t/g+) have been reported in 2′-OMe inhibited crystal structures of the hammerhead[75,76] and *glmS* ribozymes.[77,78] It should be noted that these and other RNA crystal structures are typically obtained with only medium resolution (∼2 Å) so that it is possible that such fine structural details are beyond the current refinement accuracy.[14]

The reactive conformation predicted by the *ff*99bsc0$\chi_{OL3}\varepsilon\zeta_{OL1}$ force field for the hairpin ribozyme active site features two H-bonds between the catalytically important G8 and the scissile phosphate, namely G8(N1H)···A-1(O2′) and G8(N2H)···G+1(pro-S_P). The other catalytically essential active site nucleotide, A38H$^+$, forms two additional H-bonds to the scissile phosphate, A38H$^+$(N1H)···G+1(O5′) and A38H$^+$(N6H)···G+1(pro-R_P). All four of these interactions, together with the high values of the IAA (A-1(O2′)−G+1(P)−G+1(O5′)) fluctuating up to ∼170°, arrange the active site in an architecture that is structurally preorganized for the nucleophilic attack of the A-1(2′-OH) group and thus the self-cleavage reaction (see the Supporting Information for details of this reactive conformation).

Deprotonated G8$^-$ Does Not Favor the Reactive Conformation Observed in Simulations with a Canonical G8. As shown in the preceding section, simulations using a refined version of the force field (and assuming a canonical protonation state of the G8) support a geometry of the catalytic center of the hairpin ribozyme that is consistent with catalysis. Such an active site arrangement is catalytically competent for the monoanionic reaction pathway, where the proton is shuttled from the 2′-OH nucleophile toward the O5′ leaving group via a nonbridging oxygen of the scissile phosphate, whereas the canonical G8 contributes to catalysis only by electrostatic stabilization of the transition state.[51] However, the alternative combined general base (G8$^-$)/general acid (A38H$^+$) mechanism would require a reactive conformation of the active site that involves a deprotonated guanine G8$^-$. This mechanism was suggested[46] on basis of the first crystal structures, supported by recent experiments[50,52] as well as QM/MM calculations,[51,53] and is currently believed to be the biochemically most relevant. As it is difficult to imagine that guanine would become deprotonated while being bound to the nucleophile, we assume that it is deprotonated in an inactive conformation and then has to return (at least as a rare, transient conformation) to the catalytic architecture. This constitutes a so far unresolved problem, as G8$^-$ decisively departed from the catalytic center in all our simulations so far.[22]

Given the substantial improvements observed with the ε/ζ torsion correction for simulations with the canonical G8, we decided to reinvestigate the structural dynamics of G8$^-$ in the active site using the *ff*99bsc0$\chi_{OL3}\varepsilon\zeta_{OL1}$ force field. We anticipated that G8$^-$ may form H-bonds with the 2′-OH

DOI: 10.1021/jp512069n
J. Phys. Chem. B 2015, 119, 4220−4229

nucleophile and the scissile phosphate, i.e., A-1(2′-OH)···G8⁻(N1) and G8⁻(N2H)···G+1(pro-S_P), respectively. This would imply the same arrangement of the active site as revealed by our simulation with canonical G8, except for reorientation of the 2′-OH nucleophilic group (Figure 3A). However, the

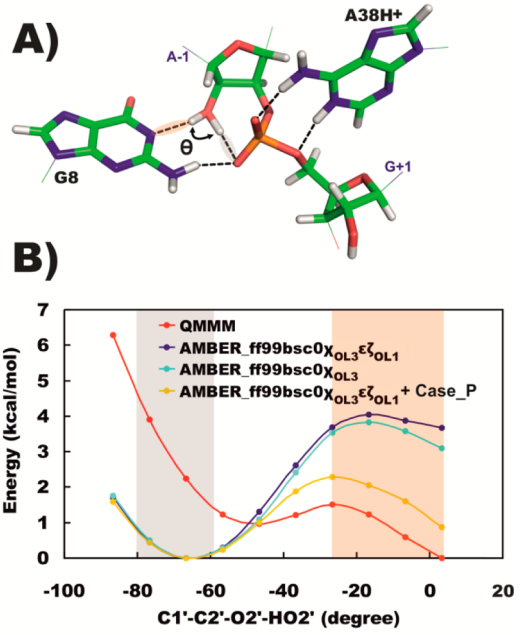

Figure 3. Comparison of the potential energy profiles along the orientation of the A-1(2′-OH) group in the hairpin ribozyme containing a deprotonated G8⁻ and a protonated A38H⁺. (A) The A-1(2′-OH) donates a H-bond to either the G+1 phosphate or the deprotonated G8⁻. (B) The QM/MM calculation favors the A-1(2′-OH)···G8⁻(N1) H-bond. The MM calculations (using *ff*99bsc0χ_{OL3}, *ff*99bsc0$\chi_{OL3}\varepsilon\zeta_{OL1}$, and *ff*99bsc0$\chi_{OL3}\varepsilon\zeta_{OL1}$ with modified van der Waals parameters of the phosphate nonbridging oxygens suggested by Case et al.[70]) significantly stabilize the alternative A-1(2′-OH)···G+1(pro-S_P) H-bond and thus destabilize the binding of G8⁻ in the active site. The colored areas correspond with the orientation of the A-1(2′-OH) group (establishing either the A-1(2′-OH)···G+1(pro-S_P) (gray) or the A-1(2′-OH)···G8⁻(N1) (beige) H-bond).

*ff*99bsc0$\chi_{OL3}\varepsilon\zeta_{OL1}$ force field improved the conformational behavior of the deprotonated G8⁻ only partially. In all unrestrained simulations, the A-1(2′-OH)···G8⁻(N1) H-bond was disrupted immediately during the equilibration phase because the A-1(2′-OH) group reoriented toward the G+1(pro-S_P) nonbridging oxygen, forming the A-1(2′-OH)···G+1(pro-S_P) H-bond instead. The second key G8⁻(N2H)···G+1(pro-S_P) H-bond was also lost within the first ns of MD simulation due to reconformation of G8⁻ in the active site. This relocation was characterized by weakening of the single G8⁻(N2H)···U+2(O4) H-bond (∼3.5 Å) stabilizing the G8⁻/U+2 base pair, and by subsequent formation of a new, transient G8⁻(N2H)···A-1(O2′) H-bond. In the simulation with excess KCl salt, both G8⁻(N2H)···U+2(O4) and G8⁻(N2H)···A-1(O2′) H-bonds were broken after ∼45 ns of MD simulation and G8⁻ left the active site, subsequently residing at a distance of ∼8 Å from the scissile phosphate.

To examine the effect of ionic conditions on the expulsion of the G8⁻, we performed two additional unrestrained simulations with G8⁻ and different types or concentrations of ions, particularly one simulation with ∼0.2 M excess NaCl salt, i.e., with the same concentration but an altered type of ion, and the other using K^+ net-neutralized conditions. We found that although the behavior of G8⁻ was insensitive to the type of ion, the lower concentration of counterions in net-neutralizing conditions partially reduced the tendency of the G8⁻ to leave the active site. Namely, we found that the population of the close contact G8⁻(N1)···A-1(O2′) distance (below 3.5 Å) was 3 ± 1% and 4 ± 3% in KCl and NaCl excess salt simulations, respectively, but increased to 15 ± 5% in the simulation with K^+ net-neutralization (see Figure S2 in the Supporting Information). However, these close contacts were not necessarily accompanied by the corresponding H-bond between the two heavy atoms due to an unsuitable orientation of the 2′-OH group. In both excess salt simulations, the 2′-OH group was permanently oriented toward the G+1(pro-S_P) nonbridging oxygen, suggesting that the close contact between G8⁻(N1)···A-1(O2′) was opportunistic and stabilized by the G8⁻(N2−H)···A-1(O2′) H-bond. However, in the net-neutralized simulation we also observed a minor (2%) population of the G8⁻(N1)···A-1(O2′-H) H-bond.

To identify the interactions involved in expulsion of the deprotonated G8⁻ from the active site (besides the electrostatic repulsion between the negatively charged G8⁻ and the scissile phosphate and the electrostatic attraction between G8⁻ and cations surrounding the RNA), we performed two MD simulations with distance restraints aimed to keep G8⁻ within the active site. Harmonic restraints were applied either to the G8⁻(N2)···U+2(O4) or to the G8⁻(N1)···A-1(O2′) distance during the equilibration phase and the first 10 ns of the production part of the MD simulations. However, none of these two restrained MD simulations affected the G8⁻ behavior so that we observed similarly rapid relocation of G8⁻ from the active site as in the unrestrained MD simulation with G8⁻ (see the Supporting Information for details of the setup and results of these MD simulations). Nevertheless, the simulations strongly suggested that the first event in the chain of rearrangements is a reorientation of A-1(2′-OH) toward the G+1(pro-S_P) nonbridging oxygen. This appears to initiate the vigorous expulsion of the G8⁻ due to disruption of the A-1(2′-OH)···G8⁻(N1) H-bond and its replacement by repulsive interaction between G8⁻(N1) and A-1(O2′), which is further amplified by the attractive interaction between G8⁻ and the cations surrounding the polyanionic RNA. This indicated that there may be additional force field imbalances at work in the catalytic center that bias the simulations and cause swift overpowering of the catalytic H-bond by the intrastrand sugar−phosphate H-bond. Therefore, subsequent calculations focused on the architectural role of the A-1(2′-OH) group within the active site.

QM/MM Calculations Reveal Sizable Error in the MM Description of the A-1(2′-OH) Orientation in the Catalytic Core of the Hairpin Ribozyme. In all our MD simulations we observed that the A-1(2′-OH) functional group generally favored an orientation toward the G+1(pro-S_P) nonbridging oxygen rather than the G8⁻(N1) nitrogen (notably, in simulations with both G8⁻ and excess salt this preference was absolute). The A-1(2′-OH)···G+1(pro-S_P) interaction was the dominant H-bond during extended MD simulations with both canonical G8 and deprotonated G8⁻. We note that, due to the nonpolarizable nature of the force field, an accurate description of interactions involving two closely spaced polarizable anions (G8⁻ and phosphate) may represent a particular force field challenge. To further check the accuracy of the force field description of conformational substates of the

DOI: 10.1021/jp512069n
J. Phys. Chem. B 2015, 119, 4220−4229

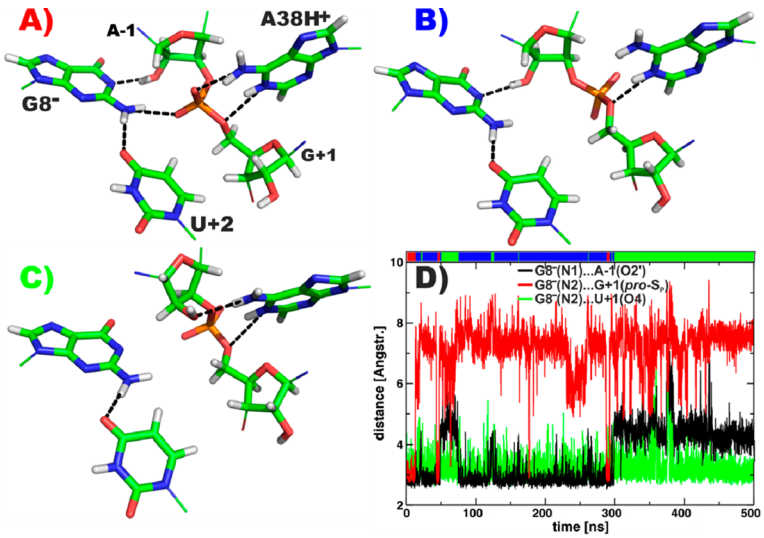

Figure 4. Conformational behavior of the *ff*99bsc0$\chi_{OL3}\varepsilon\zeta_{OL1}$ simulation with deprotonated G8$^-$ and restrained orientation of the A-1(2′-OH) toward the Watson−Crick edge of G8$^-$. (A) Reactive conformation of the active site, (B) the conformation with flipped scissile phosphate, and (C) the conformation with flipped phosphate and repuckered A-1 ribose. (D) The course of the crucial H-bonds: G8$^-$(N1)···A-1(2′-OH) in black, G8$^-$(N2H)···G+1(pro-S$_P$) in red, and G8$^-$(N2H)···U+2(O4) in green. The conformational states corresponding to panels A, B, and C are denoted via the bar diagram situated above the graph in red, blue, and green, respectively.

A-1(2′-OH) functional group (Figure 3A), we performed flexible energy scans along the A-1(C1′)−A-1(C2′)−A-1(O2′)−A-1(HO2′) dihedral using both the empirical potential and the QM DFT approach (see Methods for details). The DFT description is expected to be significantly more accurate than the approximate empirical force field, allowing us to use it as a benchmark to test the validity of the force field description of the conformation preferences of the A-1(2′-OH).

The QM/MM calculations predicted an orientation with the A-1(2′-OH) donating a H-bond to the N1 nitrogen of G8$^-$ to be the most stable. In contrast, the empirical force field consistently showed a very different preference toward the G+1(pro-S$_P$) nonbridging oxygen (Figure 3A,B). These results indicate an influence of some force field imbalances that significantly bias the conformational behavior of the A-1(2′-OH) in the presence of the deprotonated G8$^-$.

We speculated that such an imbalance may be caused by an inaccurate parametrization of the van der Waals terms and their influence on the accuracy of H-bonding interactions. To test this hypothesis, we performed an additional MM scan using modified van der Waals parameters for the phosphate oxygens. Specifically, we used the reparametrization of these van der Waals parameters as suggested by Case et al. for phosphorylated amino acids.[70] Case et al. found that the phosphate oxygens were (at least in the case of phosphorylated amino acids) too small in contemporary force fields, and a larger van der Waals radius resulted in a better description of their solvation energies.[70] We thus transferred these parameters to RNA and found that they indeed improve the MM profile but are not sufficient to entirely conform the orientation preference of the 2′-OH to that found in our benchmark QM/MM analysis (Figure 3B). Thus, a more detailed analysis of the origin of this imbalance is warranted before any force field corrections are introduced. In addition we would like to stress that the modified van der Waals parameters are not directly applicable to MD simulations as they may significantly affect torsional profiles via 1−4 van der Waals interactions. More specifically, the modified van der Waals parameters of phosphate oxygens will affect α, γ, δ, and ζ torsions.

G8$^-$ Keeps Its Reactive Conformation Once A-1(2′-OH) Is Properly Positioned toward It. As a practical solution for the observed force field deficiency in the description of the A-1(2′-OH) orientation in the presence of the deprotonated G8$^-$, we restrained the A-1(C1′)−A-1(C2′)−A-1(O2′)−A-1(HO2′) dihedral (see the Supporting Information for details) to examine the conformational behavior of G8$^-$ with the A-1(2′-OH) group oriented toward its Watson−Crick edge (as suggested by our benchmark QM/MM DFT calculations, Figure 3A). The restraint was sufficient to maintain the reactive conformation of G8$^-$. Once the restraint was released (after 10 ns), the A-1(2′-OH) immediately reoriented (as expected) toward the scissile phosphate and G8$^-$ moved out of the active site, as in the unrestrained simulation. In contrast, when we kept the dihedral restraint for the entire simulation (in this particular case we extended the simulation to 500 ns), the active site preserved a stable contact between the deprotonated G8$^-$ and the backbone around the scissile phosphate, represented by the A-1(2′-OH)···G8$^-$(N1) H-bond and transient G8$^-$(N2H)···G+1(pro-S$_P$) H-bond (Figure 4A,D). However, the reactive conformation was maintained for only ∼13 ns, after which we observed a flip of the scissile phosphate, presumably caused by the electrostatic repulsion between G8$^-$ and the phosphate (Figure 4B,D). The phosphate reconformation was similar to that described above for the *ff*99bsc0χ_{OL3} simulation with canonical G8 and restrained A-1 C2′-endo pucker (Figure 2A). This phosphate flip was accompanied by disruption of the G8$^-$(N2H)···G+1(pro-S$_P$) and A38H$^+$(N6H)···G+1(pro-R$_P$) H-bonds. The phosphate transiently flipped back and reestablished the reactive conformation of the active site for ∼5 ns but then remained flipped for the remainder of the simulation. Notably, we also observed repuckering from C2′-endo to C3′-endo sugar similar to that observed in the *ff*99bsc0χ_{OL3} simulation with canonical G8 (Figure 4C,D). However, the deprotonated G8$^-$ remained situated in its position in the active site and was capable of

DOI: 10.1021/jp512069n
J. Phys. Chem. B 2015, 119, 4220−4229

reestablishing its A-1(2′-OH)···G8$^-$(N1) H-bond when the A-1 sugar pucker returned to C2′-endo (Figure 4D).

We need to emphasize that the discrepancy between QM/MM and MM energy profiles of the A-1(2′-OH) hydroxyl rotation does not necessarily imply incorrect parametrization of the hydroxyl group dihedral term of the force field. The overall energy profile is also affected by the nonbonded terms as shown by the partial improvement observed with modified van der Waals parameters for the nonbridging phosphate oxygens. The error may be specific for the catalytic core of the hairpin ribozyme conformation, including its unusual backbone conformation. Correcting such problems by force field modifications is not straightforward, and it is not even certain whether a generally valid (i.e., broadly applicable) correction exists within the simple formalism of presently used force fields.

CONCLUSIONS

The preceding MD simulations of the hairpin ribozyme indicate two problems in the accurate description of its catalytic center: (i) inability of the force field to stabilize reactive conformation of the scissile phosphate and (ii) instability of the G8$^-$ in the catalytic center.

The first problem can be, in the presence of canonical G8, eliminated by adding the $\varepsilon\zeta_{OL1}$ correction of ε/ζ torsion angles[62] to the current standard AMBER RNA *ff*99bsc0χ_{OL3} force field. The RNA self-cleavage reaction requires a rare noncanonical conformation of the scissile sugar−phosphate backbone. As empirical force fields are primarily designed to describe canonical regions,[31] a description of noncanonical RNA conformations is challenging. In the case of the conformational behavior of the scissile phosphate, key parameters are the dihedrals affecting the ribose pucker and ε/ζ torsions. As we found that the ribose pucker is a rather passive structural parameter, an accurate parametrization of the ε/ζ torsions appears to be essential for MD simulations of ribozymes. With the *ff*99bsc0$\chi_{OL3}\varepsilon\zeta_{OL1}$ force field version we for the first time achieved a stable population of a reactive active site conformation of the hairpin ribozyme, particularly with high IAA in the catalytic ground state on the submicrosecond time scale. Such a conformation is fully compatible with the monoanionic reaction pathway, where a canonical G8 is involved in electrostatic stabilization of the transition state.

The alternative mechanism in which G8 acts as a general base would require deprotonation of G8. We found that the instability of G8$^-$ in the catalytic center remains a problem even when the *ff*99bsc0$\chi_{OL3}\varepsilon\zeta_{OL1}$ force field is used. It is worth noting that the observed instability of the G8$^-$(N1)···A-1(O2′-H) H-bond may not necessarily represent a force field artifact as we cannot rule out the possibility that G8$^-$ is not fully stable within the hairpin ribozyme active site, due to its repulsion from the like-charged scissile phosphate, and a reactive conformation with G8$^-$ ready to activate the 2′-OH nucleophile may occur only transiently. Nevertheless, reference QM/MM computations revealed a sizable bias in MM description of the interaction between the deprotonated G8$^-$ nucleobase and the scissile phosphate. The nucleophilic A-1(2′-OH) group clearly favors the G+1(pro-S_P) nonbridging oxygen as the proton acceptor during MD simulations as well as in MM scans with both canonical and deprotonated states of G8. Thus, the conformational state with the A-1(2′-OH)···G+1(pro-S_P) H-bond is significantly (and incorrectly) favored by the empirical force field over the state with the A-1(2′-OH)···G8$^-$(N1) H-bond. We propose that this imbalance most likely contributes to the observed expulsion of the deprotonated G8$^-$ from the active site in MD simulations, even with the best state-of-the-art force field. If this is true, this conformational aberration is caused by a yet-unidentified deficiency in force field parametrization. It is unlikely that such an imbalance is caused primarily by the corresponding dihedral term of the force field. It instead may be related to certain van der Waals parameters or a lack of polarization energy terms, as we observed a significant, albeit incomplete, improvement of the energy profiles of the 2′-OH orientation upon adaptation of the phosphate van der Waals parameters suggested by Case and co-workers.[70] Development and testing of an adequate correction is a very complex task that is clearly beyond the scope of the current work. A partial ad hoc improvement of such a conformational behavior is obtained by imposing a specific restraint on the A-1(2′-OH) group dihedral term, together with application of the *ff*99bsc0$\chi_{OL3}\varepsilon\zeta_{OL1}$ force field.

In summary, we suggest that the improvement of the architecture of the hairpin ribozyme's catalytic core through the *ff*99bsc0$\chi_{OL3}\varepsilon\zeta_{OL1}$ force field version is significant and represents an important step toward an optimal description of the reactive conformation of the active site in the presence of a catalytically important guanine, both in deprotonated G8$^-$ and in canonical G8 forms, corresponding to the general base and electrostatic stabilization roles of the G8, respectively. It should be noted, however, that the $\varepsilon\zeta_{OL1}$ correction has been primarily developed for DNA and, although its transfer to RNA appears promising, extensive testing for a much wider range of RNA systems will be necessary to establish ranges of its applicability to RNA simulations. An accurate description of G8$^-$ in the catalytic center of the hairpin ribozyme remains a particular challenge.

ASSOCIATED CONTENT

Supporting Information

Details about restrained MD simulations with G8$^-$, comparison of the ε/ζ torsional contributions in the *ff*99 and $\varepsilon\zeta_{OL1}$ corrected force fields, evolution of G8$^-$(N1)···A-1(O2′) distances under different ionic conditions, and two structures showing the starting snapshot for our QM/MM calculations and the modeled reactive state of the hairpin ribozyme. This material is available free of charge via the Internet at http://pubs.acs.org/.

AUTHOR INFORMATION

Corresponding Author

*P.B. Telephone: +420 585634769. E-mail: pavel.banas@upol.cz.

Notes

The authors declare no competing financial interest.

ACKNOWLEDGMENTS

This work was supported by grant P208/12/1878 (J.S., M.O., V.M., and P.K.) from the Czech Science Foundation, by the "CEITEC − Central European Institute of Technology" project CZ.1.05/1.1.00/02.0068 from the European Regional Development Fund (J.S.), Operational Program Research and Development for Innovations − European Regional Development Fund (project CZ.1.07/2.3.00/20.0058) and project LO1305 of the Ministry of Education, Youth and Sports of the Czech Republic (V.M., M.O., P.B.), by student project IGA_PrF_2014023 of

DOI: 10.1021/jp512069n
J. Phys. Chem. B 2015, 119, 4220−4229

Palacky University (V.M.), and by NIH grant GM62357 (N.G.W.).

REFERENCES

(1) Fedor, M. J.; Williamson, J. R. The Catalytic Diversity of RNAs. *Nat. Rev. Mol. Cell Biol.* **2005**, *6*, 399−412.
(2) Lilley, D. M. The Origins of RNA Catalysis in Ribozymes. *Trends Biochem. Sci.* **2003**, *28*, 495−501.
(3) Lilley, D. M. Mechanisms of RNA Catalysis. *Philos. Trans. R. Soc., B* **2011**, *366*, 2910−2917.
(4) Johnson-Buck, A. E.; McDowell, S. E.; Walter, N. G. Metal Ions: Supporting Actors in the Playbook of Small Ribozymes. *Met. Ions Life Sci.* **2011**, *9*, 175−196.
(5) Doudna, J. A.; Cech, T. R. The Chemical Repertoire of Natural Ribozymes. *Nature* **2002**, *418*, 222−228.
(6) Doudna, J. A.; Lorsch, J. R. Ribozyme Catalysis: Not Different, Just Worse. *Nat. Struct. Mol. Biol.* **2005**, *12*, 395−402.
(7) Chen, X.; Li, N.; Ellington, A. D. Ribozyme Catalysis of Metabolism in the RNA World. *Chem. Biodiversity* **2007**, *4*, 633−655.
(8) Scott, W. G. Ribozymes. *Curr. Opin. Struct. Biol.* **2007**, *17*, 280−286.
(9) Spitale, R. C.; Wedekind, J. E. Exploring Ribozyme Conformational Changes with X-ray Crystallography. *Methods* **2009**, *49*, 87−100.
(10) Fedor, M. J. Comparative Enzymology and Structural Biology of RNA Self-Cleavage. *Annu. Rev. Biophys.* **2009**, *38*, 271−299.
(11) Rhodes, M. M.; Reblova, K.; Sponer, J.; Walter, N. G. Trapped Water Molecules are Essential to Structural Dynamics and Function of a Ribozyme. *Proc. Natl. Acad. Sci. U. S. A.* **2006**, *103*, 13380−13385.
(12) Ditzler, M. A.; Sponer, J.; Walter, N. G. Molecular Dynamics Suggest Multifunctionality of an Adenine Imino Group in Acid-base Catalysis of the Hairpin Ribozyme. *RNA* **2009**, *15*, 560−575.
(13) Spitale, R. C.; Volpini, R.; Heller, M. G.; Krucinska, J.; Cristalli, G.; Wedekind, J. E. Identification of an Imino Group Indispensable for Cleavage by a Small Ribozyme. *J. Am. Chem. Soc.* **2009**, *131*, 6093−6095.
(14) Kapral, G. J.; Jain, S.; Noeske, J.; Doudna, J. A.; Richardson, D. C.; Richardson, J. S. New Tools Provide a Second Look at HDV Ribozyme Structure, Dynamics and Cleavage. *Nucleic Acids Res.* **2014**, *42*, 12833−12846.
(15) Auffinger, P.; Westhof, E. Simulations of the Molecular Dynamics of Nucleic Acids. *Curr. Opin. Struct. Biol.* **1998**, *8*, 227−236.
(16) Norberg, J.; Nilsson, L. Molecular Dynamics Applied to Nucleic Acids. *Acc. Chem. Res.* **2002**, *35*, 465−472.
(17) Cheatham, T. E. Simulation and Modeling of Nucleic Acid Structure, Dynamics and Interactions. *Curr. Opin. Struct. Biol.* **2004**, *14*, 360−367.
(18) Auffinger, P.; Hashem, Y. Nucleic Acid Solvation: From Outside to Insight. *Curr. Opin. Struct. Biol.* **2007**, *17*, 325−333.
(19) McDowell, S. E.; Spackova, N.; Sponer, J.; Walter, N. G. Molecular Dynamics Simulations of RNA: An in Silico Single Molecule Approach. *Biopolymers* **2007**, *85*, 169−184.
(20) Ditzler, M. A.; Otyepka, M.; Sponer, J.; Walter, N. G. Molecular Dynamics and Quantum Mechanics of RNA: Conformational and Chemical Change We Can Believe in. *Acc. Chem. Res.* **2010**, *43*, 40−47.
(21) Estarellas, C.; Otyepka, M.; Koča, J.; Banáš, P.; Krepl, M.; Šponer, J. Molecular Dynamic Simulations of Protein/RNA Complexes: CRISPR/Csy4 Endoribonuclease. *Biochim. Biophys. Acta* **2014**, DOI: 10.1016/j.bbagen.2014.10.021.
(22) Mlynsky, V.; Banas, P.; Hollas, D.; Reblova, K.; Walter, N. G.; Sponer, J.; Otyepka, M. Extensive Molecular Dynamics Simulations Showing that Canonical G8 and Protonated A38H$^+$ Forms are Most Consistent with Crystal Structures of Hairpin Ribozyme. *J. Phys. Chem. B* **2010**, *114*, 6642−6652.
(23) Banas, P.; Walter, N. G.; Sponer, J.; Otyepka, M. Protonation States of the Key Active Site Residues and Structural Dynamics of the *glmS* Riboswitch as Revealed by Molecular Dynamics. *J. Phys. Chem. B* **2010**, *114*, 8701−8712.
(24) Veeraraghavan, N.; Ganguly, A.; Golden, B. L.; Bevilacqua, P. C.; Hammes-Schiffer, S. Mechanistic Strategies in the HDV Ribozyme: Chelated and Diffuse Metal Ion Interactions and Active Site Protonation. *J. Phys. Chem. B* **2011**, *115*, 8346−8357.
(25) Chen, J.; Ganguly, A.; Miswan, Z.; Hammes-Schiffer, S.; Bevilacqua, P. C.; Golden, B. L. Identification of the Catalytic Mg^{2+} ion in the Hepatitis Delta Virus Ribozyme. *Biochemistry* **2013**, *52*, 557−567.
(26) Banas, P.; Hollas, D.; Zgarbova, M.; Jurecka, P.; Orozco, M.; Cheatham, T. E.; Sponer, J.; Otyepka, M. Performance of Molecular Mechanics Force Fields for RNA Simulations: Stability of UUCG and GNRA Hairpins. *J. Chem. Theory Comput.* **2010**, *6*, 3836−3849.
(27) Faustino, I.; Perez, A.; Orozco, M. Toward a Consensus View of Duplex RNA Flexibility. *Biophys. J.* **2010**, *99*, 1876−1885.
(28) Banas, P.; Sklenovsky, P.; Wedekind, J. E.; Sponer, J.; Otyepka, M. Molecular Mechanism of preQ$_1$ Riboswitch Action: A Molecular Dynamics Study. *J. Phys. Chem. B* **2012**, *116*, 12721−12734.
(29) Sponer, J.; Mladek, A.; Sponer, J. E.; Svozil, D.; Zgarbova, M.; Banas, P.; Jurecka, P.; Otyepka, M. The DNA and RNA Sugar-phosphate Backbone Emerges as the Key Player. An Overview of Quantum-Chemical, Structural Biology and Simulation Studies. *Phys. Chem. Chem. Phys.* **2012**, *14*, 15257−15277.
(30) Banas, P.; Jurecka, P.; Walter, N. G.; Sponer, J.; Otyepka, M. Theoretical Studies of RNA Catalysis: Hybrid QM/MM Methods and Their Comparison with MD and QM. *Methods* **2009**, *49*, 202−216.
(31) Sponer, J.; Cang, X.; Cheatham, T. E., 3rd. Molecular Dynamics Simulations of G-DNA and Perspectives on the Simulation of Nucleic Acid Structures. *Methods* **2012**, *57*, 25−39.
(32) Henriksen, N. M.; Roe, D. R.; Cheatham, T. E., 3rd Reliable Oligonucleotide Conformational Ensemble Generation in Explicit Solvent for Force Field Assessment Using Reservoir Replica Exchange Molecular Dynamics Simulations. *J. Phys. Chem. B* **2013**, *117*, 4014−4027.
(33) Kuhrova, P.; Banas, P.; Best, R. B.; Sponer, J.; Otyepka, M. Computer Folding of RNA Tetraloops? Are We There Yet? *J. Chem. Theory Comput.* **2013**, *9*, 2115−2125.
(34) Murray, J. B.; Seyhan, A. A.; Walter, N. G.; Burke, J. M.; Scott, W. G. The Hammerhead, Hairpin and VS Ribozymes are Catalytically Proficient in Monovalent Cations Alone. *Chem. Biol.* **1998**, *5*, 587−595.
(35) Fedor, M. J. Structure and Function of the Hairpin Ribozyme. *J. Mol. Biol.* **2000**, *297*, 269−291.
(36) Pinard, R.; Hampel, K. J.; Heckman, J. E.; Lambert, D.; Chan, P. A.; Major, F.; Burke, J. M. Functional Involvement of G8 in the Hairpin Ribozyme Cleavage Mechanism. *EMBO J.* **2001**, *20*, 6434−6442.
(37) Rupert, P. B.; Ferre-D'Amare, A. R. Crystal Structure of a Hairpin Ribozyme-inhibitor Complex with Implications for Catalysis. *Nature* **2001**, *410*, 780−786.
(38) Rupert, P. B.; Massey, A. P.; Sigurdsson, S. T.; Ferre-D'Amare, A. R. Transition State Stabilization by a Catalytic RNA. *Science* **2002**, *298*, 1421−1424.
(39) Lebruska, L. L.; Kuzmine, I. I.; Fedor, M. J. Rescue of an Abasic Hairpin Ribozyme by Cationic Nucleobases: Evidence for a Novel Mechanism of RNA Catalysis. *Chem. Biol.* **2002**, *9*, 465−473.
(40) Kuzmin, Y. I.; Da Costa, C. P.; Fedor, M. J. Role of an Active Site Guanine in Hairpin Ribozyme Catalysis Probed by Exogenous Nucleobase Rescue. *J. Mol. Biol.* **2004**, *340*, 233−251.
(41) Kuzmin, Y. I.; Da Costa, C. P.; Cottrell, J. W.; Fedor, M. J. Role of an Active Site Adenine in Hairpin Ribozyme Catalysis. *J. Mol. Biol.* **2005**, *349*, 989−1010.
(42) Cottrell, J. W.; Kuzmin, Y. I.; Fedor, M. J. Functional Analysis of Hairpin Ribozyme Active Site Architecture. *J. Biol. Chem.* **2007**, *282*, 13498−13507.
(43) Ditzler, M. A.; Rueda, D.; Mo, J. J.; Hakansson, K.; Walter, N. G. A Rugged Free Energy Landscape Separates Multiple Functional RNA Folds throughout Denaturation. *Nucleic Acids Res.* **2008**, *36*, 7088−7099.

DOI: 10.1021/jp512069n
J. Phys. Chem. B 2015, 119, 4220−4229

(44) Liu, L.; Cottrell, J. W.; Scott, L. G.; Fedor, M. J. Direct Measurement of the Ionization State of an Essential Guanine in the Hairpin Ribozyme. *Nat. Chem. Biol.* **2009**, *5*, 351−357.
(45) Cottrell, J. W.; Scott, L. G.; Fedor, M. J. The pH Dependence of Hairpin Ribozyme Catalysis Reflects Ionization of an Active Site Adenine. *J. Biol. Chem.* **2011**, *286*, 17658−17664.
(46) Bevilacqua, P. C. Mechanistic Considerations for General Acid-base Catalysis by RNA: Revisiting the Mechanism of the Hairpin Ribozyme. *Biochemistry* **2003**, *42*, 2259−2265.
(47) Nam, K.; Gao, J. L.; York, D. M. Electrostatic Interactions in the Hairpin Ribozyme Account for the Majority of the Rate Acceleration without Chemical Participation by Nucleobases. *RNA* **2008**, *14*, 1501−1507.
(48) Nam, K. H.; Gao, J. L.; York, D. M. Quantum Mechanical/Molecular Mechanical Simulation Study of the Mechanism of Hairpin Ribozyme Catalysis. *J. Am. Chem. Soc.* **2008**, *130*, 4680−4691.
(49) Guo, M.; Spitale, R. C.; Volpini, R.; Krucinska, J.; Cristalli, G.; Carey, P. R.; Wedekind, J. E. Direct Raman Measurement of an Elevated Base pK_a in the Active Site of a Small Ribozyme in a Precatalytic Conformation. *J. Am. Chem. Soc.* **2009**, *131*, 12908−12909.
(50) Wilson, T. J.; Lilley, D. M. Do the Hairpin and VS Ribozymes Share a Common Catalytic Mechanism Based on General Acid-base Catalysis? A Critical Assessment of Available Experimental Data. *RNA* **2011**, *17*, 213−221.
(51) Mlynsky, V.; Banas, P.; Walter, N. G.; Sponer, J.; Otyepka, M. QM/MM Studies of Hairpin Ribozyme Self-Cleavage Suggest the Feasibility of Multiple Competing Reaction Mechanisms. *J. Phys. Chem. B* **2011**, *115*, 13911−13924.
(52) Kath-Schorr, S.; Wilson, T. J.; Li, N. S.; Lu, J.; Piccirilli, J. A.; Lilley, D. M. General Acid-base Catalysis Mediated by Nucleobases in the Hairpin Ribozyme. *J. Am. Chem. Soc.* **2012**, *134*, 16717−16724.
(53) Mlynsky, V.; Banas, P.; Sponer, J.; van der Kamp, M. W.; Mulholland, A. J.; Otyepka, M. Comparison of ab Initio, DFT, and Semiempirical QM/MM Approaches for Description of Catalytic Mechanism of Hairpin Ribozyme. *J. Chem. Theory Comput.* **2014**, *10*, 1608−1622.
(54) Alam, S.; Grum-Tokars, V.; Krucinska, J.; Kundracik, M. L.; Wedekind, J. E. Conformational Heterogeneity at Position U37 of an All-RNA Hairpin Ribozyme with Implications for Metal Binding and the Catalytic Structure of the S-turn. *Biochemistry* **2005**, *44*, 14396−14408.
(55) Salter, J.; Krucinska, J.; Alam, S.; Grum-Tokars, V.; Wedekind, J. E. Water in the Active Site of an All-RNA Hairpin Ribozyme and Effects of Gua8 Base Variants on the Geometry of Phosphoryl Transfer. *Biochemistry* **2006**, *45*, 686−700.
(56) Macelrevey, C.; Salter, J. D.; Krucinska, J.; Wedekind, J. E. Structural Effects of Nucleobase Variations at Key Active Site Residue Ade38 in the Hairpin Ribozyme. *RNA* **2008**, *14*, 1600−1616.
(57) Cornell, W. D.; Cieplak, P.; Bayly, C. I.; Gould, I. R.; Merz, K. M.; Ferguson, D. M.; Spellmeyer, D. C.; Fox, T.; Caldwell, J. W.; Kollman, P. A. A Second Generation Force Field for the Simulation of Proteins, Nucleic Acids, and Organic Molecules. *J. Am. Chem. Soc.* **1995**, *117*, 5179−5197.
(58) Wang, J. M.; Cieplak, P.; Kollman, P. A. How Well Does a Restrained Electrostatic Potential (RESP) Model Perform in Calculating Conformational Energies of Organic and Biological Molecules? *J. Comput. Chem.* **2000**, *21*, 1049−1074.
(59) Perez, A.; Marchan, I.; Svozil, D.; Sponer, J.; Cheatham, T. E.; Laughton, C. A.; Orozco, M. Refinement of the AMBER Force Field for Nucleic Acids: Improving the Description of Alpha/Gamma Conformers. *Biophys. J.* **2007**, *92*, 3817−3829.
(60) Sponer, J.; Banas, P.; Jurecka, P.; Zgarbova, M.; Kuhrova, P.; Havrila, M.; Krepl, M.; Stadlbauer, P.; Otyepka, M. Molecular Dynamics Simulations of Nucleic Acids. From Tetranucleotides to the Ribosome. *J. Phys. Chem. Lett.* **2014**, *5*, 1771−1782.
(61) Zgarbova, M.; Otyepka, M.; Sponer, J.; Mladek, A.; Banas, P.; Cheatham, T. E., 3rd; Jurecka, P. Refinement of the Cornell et al. Nucleic Acids Force Field Based on Reference Quantum Chemical Calculations of Glycosidic Torsion Profiles. *J. Chem. Theory Comput.* **2011**, *7*, 2886−2902.
(62) Zgarbova, M.; Luque, F. J.; Sponer, J.; Cheatham, T. E., 3rd; Otyepka, M.; Jurecka, P. Toward Improved Description of DNA Backbone: Revisiting Epsilon and Zeta Torsion Force Field Parameters. *J. Chem. Theory Comput.* **2013**, *9*, 2339−2354.
(63) Aqvist, J. Ion Water Interaction Potentials Derived from Free-Energy Perturbation Simulations. *J. Phys. Chem.* **1990**, *94*, 8021−8024.
(64) Joung, I. S.; Cheatham, T. E. Determination of Alkali and Halide Monovalent Ion Parameters for Use in Explicitly Solvated Biomolecular Simulations. *J. Phys. Chem. B* **2008**, *112*, 9020−9041.
(65) Berendsen, H. J. C.; Postma, J. P. M.; Vangunsteren, W. F.; Dinola, A.; Haak, J. R. Molecular-Dynamics with Coupling to an External Bath. *J. Chem. Phys.* **1984**, *81*, 3684−3690.
(66) Svensson, M.; Humbel, S.; Froese, R. D. J.; Matsubara, T.; Sieber, S.; Morokuma, K. ONIOM: A Multilayered Integrated MO +MM Method for Geometry Optimizations and Single Point Energy Predictions. A test for Diels-Alder Reactions and $Pt(P(t\text{-}Bu)_3)_2+H_2$ Oxidative Addition. *J. Phys. Chem.* **1996**, *100*, 19357−19363.
(67) Frisch, M. J.; Trucks, G. W.; Schlegel, H. B.; Scuseria, G. E.; Robb, M. A.; Cheeseman, J. R.; Scalmani, G.; Barone, V.; Mennucci, B.; Petersson, G. A.; et al. *Gaussian09*; Gaussian, Inc.: Wallingford, CT, USA, 2009.
(68) Lynch, B. J.; Fast, P. L.; Harris, M.; Truhlar, D. G. Adiabatic Connection for Kinetics. *J. Phys. Chem. A* **2000**, *104*, 4811−4815.
(69) Lynch, B. J.; Truhlar, D. G. How Well Can Hybrid Density Functional Methods Predict Transition State Geometries and Barrier Heights? *J. Phys. Chem. A* **2001**, *105*, 2936−2941.
(70) Steinbrecher, T.; Latzer, J.; Case, D. A. Revised AMBER Parameters for Bioorganic Phosphates. *J. Chem. Theory Comput.* **2012**, *8*, 4405−4412.
(71) Case, D. A.; Darden, T. A.; Cheatham, T. E. I.; Simmerling, C. L.; Wang, J.; Duke, R. E.; Luo, R.; Walker, R. C.; Zhang, W.; Merz, K. M.; et al. *AMBER*, 12.0; University of California: San Francisco, 2012.
(72) Liberman, J. A.; Guo, M.; Jenkins, J. L.; Krucinska, J.; Chen, Y.; Carey, P. R.; Wedekind, J. E. A Transition-state Interaction Shifts Nucleobase Ionization toward Neutrality to Facilitate Small Ribozyme Catalysis. *J. Am. Chem. Soc.* **2012**, *134*, 16933−16936.
(73) Murray, L. J.; Arendall, W. B., 3rd; Richardson, D. C.; Richardson, J. S. RNA Backbone is Rotameric. *Proc. Natl. Acad. Sci. U. S. A.* **2003**, *100*, 13904−13909.
(74) Richardson, J. S.; Schneider, B.; Murray, L. W.; Kapral, G. J.; Immormino, R. M.; Headd, J. J.; Richardson, D. C.; Ham, D.; Hershkovits, E.; Williams, L. D.; et al. RNA Backbone: Consensus All-angle Conformers and Modular String Nomenclature (an RNA Ontology Consortium contribution). *RNA* **2008**, *14*, 465−481.
(75) Martick, M.; Scott, W. G. Tertiary Contacts Distant from the Active Site Prime a Ribozyme for Catalysis. *Cell* **2006**, *126*, 309−320.
(76) Anderson, M.; Schultz, E. P.; Martick, M.; Scott, W. G. Active-site Monovalent Cations Revealed in a 1.55-A-resolution Hammerhead Ribozyme Structure. *J. Mol. Biol.* **2013**, *425*, 3790−3798.
(77) Klein, D. J.; Been, M. D.; Ferre-D'Amare, A. R. Essential Role of an Active-site Guanine in glmS Ribozyme Catalysis. *J. Am. Chem. Soc.* **2007**, *129*, 14858−14859.
(78) Klein, D. J.; Wilkinson, S. R.; Been, M. D.; Ferre-D'Amare, A. R. Requirement of Helix P2.2 and Nucleotide G1 for Positioning the Cleavage Site and Cofactor of the glmS Ribozyme. *J. Mol. Biol.* **2007**, *373*, 178−189.

DOI: 10.1021/jp512069n
J. Phys. Chem. B 2015, 119, 4220−4229